

Mining for normal galaxies in the First XMM-Newton Serendipitous Source Catalog

A. E. Georgakakis^{1,2*}, V. Chavushyan^{3,4}, M. Plionis^{1,3}, I. Georgantopoulos¹,
E. Koulouridis^{1,5}, I. Leonidaki^{1,5}, A. Mercado³

¹*Institute of Astronomy & Astrophysics, National Observatory of Athens, I. Metaxa & V. Pavlou, Athens, 15236, Greece*

²*Astrophysics Group, Blackett Laboratory, Imperial College, Prince Consort Rd, London SW7 2BZ, UK*

³*Instituto Nacional de Astrofísica Óptica y Electrónica, AP 51 y 216, 72000, Puebla, Pue, México*

⁴*Instituto de Astronomía, Universidad Nacional Autónoma de México, A.P. 70-264, DF 04510, México*

⁵*Astronomical Laboratory, Department of Physics, University of Patras, 26500 Rio-Patras, Greece*

4 June 2018

ABSTRACT

This paper uses the First *XMM-Newton* Serendipitous Source Catalog compiled by the *XMM-Newton* Science Center to identify low- z X-ray selected normal galaxy candidates. Our sample covers a total area of $\approx 6 \text{ deg}^2$ to the 0.5-2 keV limit $\approx 10^{-15} \text{ erg s}^{-1} \text{ cm}^{-2}$. A total of 23 sources are selected on the basis of low X-ray-to-optical flux ratio $\log f_X/f_{opt} < -2$, soft X-ray spectral properties and optical spectra, when available, consistent with stellar than AGN processes. This sample is combined with similarly selected systems from the Needles in the Haystack Survey (Georgantopoulos et al. 2005) to provide a total of 46 unique $z \lesssim 0.2$ X-ray detected normal galaxies, the largest low- z sample yet available. This is first used to constrain the normal galaxy $\log N - \log S$ at bright fluxes ($10^{-15} - 10^{-13} \text{ erg s}^{-1} \text{ cm}^{-2}$). We estimate a slope of -1.46 ± 0.13 for the cumulative number counts consistent with the euclidean prediction. We further combine our sample with 23 local ($z \lesssim 0.2$) galaxies from the *Chandra* Deep Field North and South surveys to construct the local X-ray luminosity function of normal galaxies. A Schechter form provides a good fit to the data with a break at $\log L_* = 41.02^{+0.14}_{-0.12} \text{ erg s}^{-1}$ and a slope of $\alpha = -1.76 \pm 0.10$. Finally, for the sample of 46 systems we explore the association between X-ray luminosity and host galaxy properties, such as star-formation rate and stellar mass. We find that the L_X of the emission-line systems correlates with $H\alpha$ luminosity and 1.4 GHz radio power, both providing an estimate of the current star-formation rate. In the case of early type galaxies with absorption line optical spectra we use the K -band as proxy to stellar mass and find a correlation of the form $L_X \propto L_K^{1.5}$. This is flatter than the $L_X - L_B$ relation for local ellipticals. This may be due to either L_K providing a better proxy to galaxy mass or selection effects biasing our sample against very luminous early-type galaxies, $L_X > 10^{42} \text{ erg s}^{-1}$.

Key words: Surveys – X-rays: galaxies – X-rays: general

1 INTRODUCTION

The launch of the *XMM-Newton* and the *Chandra* missions has opened new opportunities in the study of the X-ray properties of normal galaxies. Apart from targeted observations of local systems, surveys performed by these telescopes have allowed, for the first time, study of normal galaxies at

X-ray wavelengths outside the nearby Universe, thus opening the way for evolutionary investigations. Stacking analysis studies using these missions for example, have provided constraints on the mean X-ray properties (L_X , hardness ratios, L_X/L_B) of star-forming systems over the redshift range $z = 0.1 - 3$ (Hornschemeier et al. 2002; Nandra et al. 2002; Georgakakis et al. 2003a, b; Laird et al. 2004). The stacking analysis results from the above independent studies when combined together are consistent with luminosity evolution

* email: a.georgakakis@imperial.ac.uk

of the form $\approx (1+z)^3$ at least to $z \approx 1.5$ (e.g. Georgakakis et al. 2003a, b).

The X-ray stacking analysis provides information on the mean properties of systems that are too X-ray faint to be individually detected. A major breakthrough however, of the *XMM-Newton* and the *Chandra* missions has been the *detection* of normal galaxies at low and moderate redshifts. Bauer et al. (2002) and Alexander et al. (2002) studied the radio and mid-infrared properties of X-ray sources in the Chandra Deep Field (CDF) North and argue that systems with X-ray emission dominated by starburst activity are detected in this field out to $z \approx 1$. Hornschemeier et al. (2003) demonstrated that more quiescent normal galaxies with X-ray-to-optical flux ratio $\log f_X/f_{opt} < -2$ and a median redshift $z \approx 0.3$ not only constitute a non-negligible component of the X-ray source population in the CDF-North but are also likely to outnumber AGNs at fluxes below $f_X(0.5-2 \text{ keV}) \approx 10^{-17} \text{ erg s}^{-1} \text{ cm}^{-2}$. Norman et al. (2004) extended the Hornschemeier et al. (2003) study and identified over 100 starburst/quiescent galaxy candidates to $z \approx 1$ in the combined CDF-North and South albeit with optical spectroscopy limited to a fraction of them. These authors estimate the X-ray luminosity function of normal galaxy candidates and find evidence for X-ray evolution of the form $\propto (1+z)^3$ to $z \approx 1$, i.e. similar to that inferred from other wavelengths (e.g. Hopkins 2004 and references therein).

Parallel to the studies above focusing on distant sources ($z \gtrsim 0.3$), there have also been efforts to compile X-ray selected normal galaxy samples at low redshifts $z < 0.2$. This is essential to complement the deep CDF studies and to provide a comparison sample in the nearby Universe. Georgakakis et al. (2004) and Georgantopoulos, Georgakakis & Koulouridis (2005) used public *XMM-Newton* data overlapping with the Sloan Digital Sky Survey (SDSS; Stoughton et al. 2002; York et al. 2000) to identify normal galaxies at a median redshift of about 0.07 over an 11 deg^2 area. This dataset, the Needles in the Haystack Survey, has been used to constrain the galaxy $\log N - \log S$ at bright fluxes, estimate the X-ray luminosity function of absorption and emission line galaxies separately and to assess their contribution to the diffuse X-ray background under different evolution scenarios. A similar study using the HRI detector onboard *ROSAT* has been performed by Tajer et al. (2005) aiming to determine the number counts of low X-ray-to-optical flux ratio systems ($\log f_X/f_{opt} < -1$) at very bright fluxes ($10^{-14} - 10^{-12} \text{ erg s}^{-1} \text{ cm}^{-2}$). More recently, Hornschemeier et al. (2005) explored the X-ray properties of $z \approx 0.1$ galaxies identified in public *Chandra* pointings overlapping with the SDSS. They use this sample to investigate the link between X-ray luminosity, host galaxy star-formation rate (SFR) and stellar mass. These relations are consistent with a picture where the X-ray emission arises in a combination of low- and high-mass X-ray binaries as well as hot gas interstellar medium.

Despite significance progress, the number of X-ray selected normal galaxies at low- z (e.g. $z \lesssim 0.2$) remains small hampering statistical studies. In this paper we further expand existing samples using as a resource the 1st *XMM-Newton* Serendipitous Source Catalogue produced by the *XMM-Newton* Science Center. Our aim is to demonstrate the power of this unique and continuously expanding database and how it can be exploited to advance our under-

standing of the properties of X-ray selected normal galaxies. Among others, such a sample can provide a tight anchor point for comparison with deeper surveys probing on average higher- z , calibrate the relation between SFR diagnostics and X-ray luminosity and improve our understanding of the association between host galaxy properties (e.g. stellar mass) and X-ray emission. Throughout this paper we adopt $H_0 = 70 \text{ km s}^{-1} \text{ Mpc}^{-1}$, $\Omega_M = 0.3$ and $\Omega_\Lambda = 0.7$.

2 SAMPLE SELECTION AND OBSERVATIONS

2.1 The X-ray data

In this paper we use the First *XMM-Newton* Serendipitous Source Catalogue (1 XMM; version 1.0.1) constructed by the *XMM-Newton* Survey Science Centre (SSC[†]) and released on 2003 April 7th. This is a huge database comprising source detections drawn from 585 *XMM-Newton* EPIC observations made between 2000 March 1 and 2002 May 5.

After the initial reduction of the raw data and the filtering of the high particle background periods the resulting event files are used to construct images in 5 energy bands: 0.2–0.5, 0.5–2.0, 2.0–4.5, 4.5–7.5 and 7.5–12.0 keV. The initial source detection is performed simultaneously on the 5 energy bands above using the EBOXDETECT task of SAS. The detected sources are passed on to the SAS task EMLDETECT to assess their reliability and to determine various source parameters by fitting the instrumental point spread function (PSF). The source position was fit simultaneously on all input images, whereas the source count rates are left to vary independently in each image. EMLDETECT estimates count rates corrected for vignetting, losses due to inter-chip gaps, bad pixels/columns, events arriving during readout times and the extended PSF. Parallel to the source count rate the EMLDETECT task also outputs the detection likelihood for each source providing an estimate of the probability of spurious detection. We convert count rates to flux assuming a power-law spectral energy distribution with index $\Gamma = 1.8$ and Galactic absorption appropriate for each individual *XMM-Newton* field. The index $\Gamma = 1.8$ is consistent with the median hardness ratio, $HR \approx -0.6$, of late-type galaxies in our final sample (see section 3). Using a Raymond-Smith model with a temperature of 1 keV instead of a power-law, would overestimate the flux in the 0.5–2 keV band by only about 4 per cent.

In this paper we concentrate on *XMM-Newton* fields that have the EPIC (European Photon Imaging Camera; Strüder et al. 2001; Turner et al. 2001) cameras as the prime instrument with the PN detector operated in full-frame mode and exposure times > 7 ks, to avoid observations that are too shallow to be useful for our purposes. We consider only sources with declination $\text{DEC}(J2000) > -10 \text{ deg}$ to guarantee access from northern hemisphere telescopes and galactic latitude $|b_{\text{II}}| > 20 \text{ deg}$ to minimise contamination from Galactic stars. We use sources detected on the 0.5–2 keV PN images (i.e. we do not consider the MOS1 and 2 CCDs here) at off-axis angles $< 14 \text{ arcmin}$, to avoid spurious sources close to the edge of the field of view.

[†] <http://xmmssc-www.star.le.ac.uk/>

Finally, in this paper we only consider fields with right ascensions, $RA(J2000) > 4$ hours, where our spectroscopic follow-up program of normal galaxy candidates is complete. For systems with $RA(J2000) = 0 - 4$ hours optical spectroscopy is in progress. A total of 51 *XMM-Newton* fields fulfil the criteria above.

A drawback of the 1XMM catalogue is that there is no areal coverage information providing an estimate of the surveyed area available at different point-source flux limits. To overpass this issue we determine the area curve indirectly by comparing the differential observed counts (i.e. including any incompleteness) in the 0.5-2 keV band with the expected $\log N - \log S$ from the literature. Here, we adopt the double-power law parametrisation of Baldi et al. (2002) for the 0.5-2 keV differential source counts. For the observed counts we use all X-ray sources in the 1XMM catalogue that overlap with the *XMM-Newton* fields considered in this paper and 0.5-2 keV likelihood probability > 7 . The comparison between our uncorrected counts and the Baldi et al. (2002) double-power law is shown in Figure 1. The resulting area curve is plotted in Figure 2. This is increasing to about 6 deg^2 at $\approx 10^{-14} \text{ erg s}^{-1} \text{ cm}^{-2}$ and then remains almost constant. At bright fluxes, $\gtrsim 10^{-13} \text{ erg s}^{-1} \text{ cm}^{-2}$, the uncorrected differential counts in Figure 1 are affected by (i) sources associated with the prime target of a given *XMM-Newton* pointing (Galactic stars or QSOs), (ii) small number statistics and (iii) uncertainties arising from the extrapolation of the Baldi et al. (2002) source counts to these fluxes. As a result the area curve above $\approx 10^{-13} \text{ erg s}^{-1} \text{ cm}^{-2}$ is unreliable. However, this does not affect our results since all our normal galaxy candidates are fainter than $10^{-13} \text{ erg s}^{-1} \text{ cm}^{-2}$ (see section 3). We also confirm that the area curve in Figure 2 is robust using the Needles in the Haystack Survey (Georgantopoulos et al. 2005). For that sample we derive the area curve using the method outlined above and compare it with that estimated using the sensitivity maps. We find excellent agreement between the two methods suggesting that the area curve in Figure 2 is reliable.

2.2 Normal galaxy selection

The SSC cross-correlates the 1XMM X-ray source positions with various astronomical catalogues including the U.S. Naval Observatory Catalog (USNO) version A2.0. This provides a homogeneous platform for the optical identification of 1XMM sources. The USNO-A2.0 catalogue is based on photographic material and provides accurate positions (typical error of ≈ 0.25 arcsec) and reasonable *B*-band photometry with typical photometric errors of about 0.25 mag (Monet et al. 2003). This photometric uncertainty is adequate for this study that identifies ‘normal’ galaxy candidates on the basis of the low X-ray-to-optical flux ratio $\log f_X/f_{opt} < -2$. This is estimated from the 0.5-2 keV flux $f_X(0.5-2 \text{ keV})$ and the USNO-A2.0 *B*-band magnitude according to the relation

$$\log \frac{f_X}{f_{opt}} = \log f(0.5-2 \text{ keV}) + 0.4B + 5.29. \quad (1)$$

The equation above is derived from the X-ray-to-optical flux ratio definition of Stocke et al. (1991) that involved 0.3-3.5 keV flux and *V*-band magnitude. These quantities

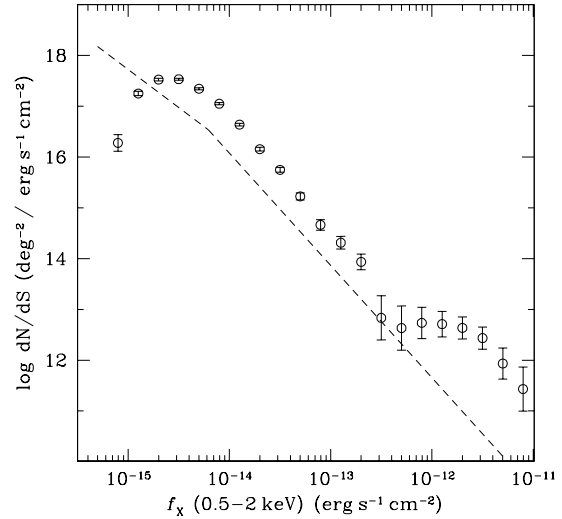


Figure 1. Differential source counts in the 0.5-2 keV band. The dots are the dN/dS for all the 1XMM catalogue sources with likelihood probability > 7 that lie on the *XMM-Newton* fields considered in this paper. The dashed line is the double power-law fit to the 0.5-2 keV counts of Baldi et al. (2002).

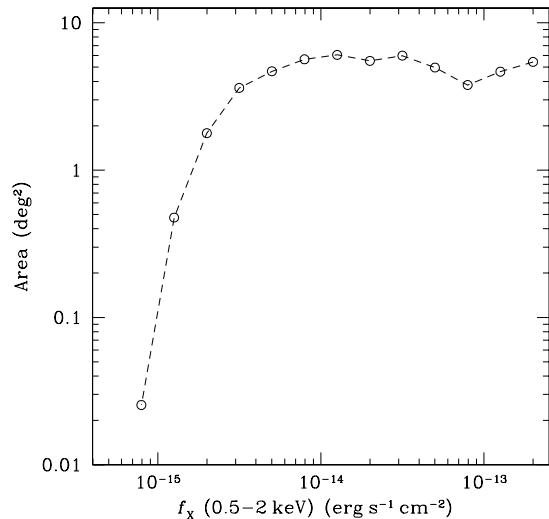


Figure 2. Solid angle as a function of limiting flux in the 0.5-2 keV band.

are converted to 0.5-2 keV flux and *B*-band magnitude assuming a mean colour $B - V = 0.8$ and a power-law X-ray spectral energy distribution with index $\Gamma = 1.8$. The $\log f_X/f_{opt} = -2$ cutoff although minimises the AGN contamination may exclude from the sample X-ray ultra-luminous normal galaxies such as powerful starbursts (e.g. NGC 3256; $\approx 2 \times 10^{42} \text{ erg s}^{-1}$; Moran, Lehnert & Helfand 1999) or very massive ellipticals ($L_X > 10^{42} \text{ erg s}^{-1}$; e.g. O’Sullivan, Forbes & Ponman 2001). Georgantopoulos et al. (2005) argue that in the case of star-forming galaxies the $\log f_X/f_{opt} = -2$ limit is not likely to be a major

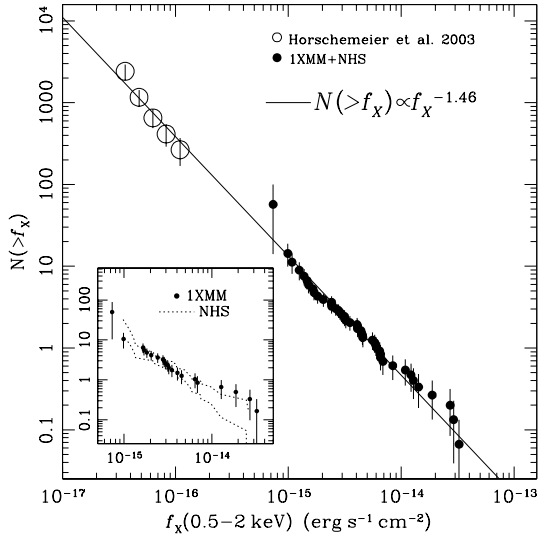


Figure 3. Cumulative normal galaxy counts in the 0.5-2 keV spectral band. Filled circles are the combined sample of normal galaxy candidates from the Needles in the Haystack Survey (NHS; Georgantopoulos et al. 2005) and the present study. The open circles are the source counts of Horschemeier et al. (2003). The continuous line is the best fit to the $\log N - \log S$ at bright fluxes from the combined NHS and 1XMM samples. The inset plot shows the $\log N - \log S$ for the galaxies in the present study only, in comparison with the counts from the NHS

source of incompleteness, at least for the low- z Universe. For early type galaxies we use the local E/S0 sample of Fabiano et al. (1992) to estimate incompleteness because of the $\log f_X/f_{opt} = -2$ cutoff. We find that about 20 per cent of the galaxies in that sample have $\log L_X/L_B > -2$, most of which are also luminous with $L_X \gtrsim 10^{42} \text{ erg s}^{-1}$. We note however, that some AGN contamination is expected within this X-ray bright subsample.

The $\log f_X/f_{opt} < -2$ regime is also populated with Galactic stars. The USNO A2.0 catalogue does not discriminate between optically extended and point-like sources. For this purpose we use the APM scans of the UKST plates[‡] that provide star/galaxy separation. We further quantify the reliability of the APM star/galaxy classification below, using follow-up spectroscopic observations or CCD quality data from the 3rd release of the Sloan Digital Sky Survey (SDSS DR3), where available.

A total of 102 sources in our 1XMM sample have $\log f_X/f_{opt} < -2$. APM classifies 69 of them point-like and 30 extended (e.g. galaxies) with the remaining 3 having ambiguous classification. The latter class is for objects that are assigned different types on the red and blue UKST survey plates.

2.3 Optical spectroscopic observations

A total of 21 out of 102 sources in our 1XMM sample with $\log f_X/f_{opt} < -2$ have been observed, 5 of them are unre-

solved in APM with the remaining 16 classified galaxy-like. The 5 point-like sources are included in the target list for follow-up spectroscopic observations to explore the reliability of the APM star/galaxy separation.

Low resolution optical spectroscopy was carried out with the Mexican 2-m class telescopes of the Observatorio Astrofisico Guillermo Haro (OAGH) in Cananea and Observatorio Astronomico Nacional de San Pedro Martir (OAN SPM). Observations with the 2.1-m OAGH telescope were carried out with the Boller & Chivens (B&Ch) spectrograph and Landessternwarte Faint Object Spectrograph and Camera (LFOSC) Zickgraf et al. (1997).

The B&Ch spectrograph uses a Tektronix TK1024AB CCD mounted at the Cassegrain focus giving a pixel scale of approximately 0.45 arcsec. We use a 2.5 arcsec wide slit and a grating with 150 lines/mm providing a dispersion of $3.5 \text{ \AA pixel}^{-1}$ and a wavelength resolution of $\approx 15 \text{ \AA}$ (≈ 4 pixels FWHM) over the range 3800–7100 \AA . The LFOSC is attached to the Cassegrain focus and is equipped with an EEV P8603 385x578 CCD giving a $10 \times 6 \text{ arcmin}^2$ field of view and an image scale of 1 arcsec. We used a 3 arcsec wide slit and the G3 grism giving a wavelength resolution of $\approx 18 \text{ \AA}$ in the range 4200–9000 \AA . The observations were carried out during various observing runs between December 2003 and March 2005.

The observations with the 2.1-m OAN-SPM telescope were carried out with the B&Ch spectrograph equipped with SITe3 (1024x1024 pix) CCD installed at the Cassegrain focus giving a pixel scale of approximately 1 arcsec. We use a 2.5 arcsec wide slit and a grating with 300 lines/mm, providing a dispersion of 4.5 \AA/pix and an effective instrumental spectral resolution of about 10 \AA (≈ 2 pixels FWHM) in the wavelength range 3800–8000 \AA . The observations were carried out during two observing runs in November 2003 and February 2004.

Typical exposure times for both the B&Ch and the LFOSC were 1 h per target. The observations were reduced following standard procedures using IRAF tasks resulting in wavelength and flux calibrated spectra. Redshifts were determined by visual inspection. Optical spectra of the galaxies from these observations are presented in Appendix 1. Our own follow-up spectroscopy is complemented with publicly available data from either the SDSS or the literature.

Out of the 30 sources classified extended by APM one is the prime target of the *XMM-Newton* pointing (NGC 3184) and one has unresolved optical light profile in the SDSS CCD quality data and therefore is most likely associated with a Galactic star. Of the remaining 28 sources a total of 26 are assigned spectroscopic redshifts from either our own campaign (17) or the literature (9). Two sources in the sample have no redshifts.

From the sources classified optically unresolved by the APM a total of 18 have either spectroscopic data from our own campaign or CCD quality star/galaxy separation from the SDSS. All these sources are indeed confirmed to be Galactic stars suggesting that the APM classification is reliable. Finally, all 3 ambiguous sources are associated with Galactic stars on the basis of the optical spectra or SDSS photometric data.

[‡] <http://www.ast.cam.ac.uk/~apmcat>

3 THE SAMPLE

In the analysis that follows we exclude all Galactic stars on the basis of either optical spectroscopy or the APM/SDSS star/galaxy separation. Our final normal galaxy sample comprises a total of 28 sources, 26 spectroscopically identified galaxies and 2 sources without spectra classified extended by APM. This is presented in Table 1. For completeness we also show the 4 sources with extended (1) or ambiguous (3) APM classification that turned out to be Galactic stars.

A number of sources in our sample are classified AGNs on the basis of their optical spectroscopic properties. These include source #A063 which is a BAL-QSO at $z = 0.149$ (Gallagher et al. 1999) and source #A140 (NGC 4156) suggested to harbor AGN activity by Elvis et al. (1981). Two of the systems for which we obtained optical spectroscopic observations, #A001 and A035 (see Fig. A1), show evidence for broad H α emission-line with FWHM $\delta v \approx 1600$ and 2000 km s^{-1} respectively. In both cases the measured broad width may be partly due to the low resolution spectrum that does not allow separation of the H α from the [N II] 6583 Å. Nevertheless, we conservatively classify these sources AGN. Source #A019 has narrow optical emission lines but the line ratios [$\log([\text{S II}] 6716 + 31/\text{H}\alpha) \approx -0.4$, $\log([\text{O III}] 5007/\text{H}\beta) \approx +0.5$; see Fig. A1] place it in the AGN region of the diagnostic diagrams of Kewley et al. (2001) first introduced by Baldwin, Phillips & Terlevich (1981) and Veilleux & Osterbrock (1987). Here we adopt the theoretical lower bound for starburst galaxy emission-line ratios from Kewley et al. (2001; see their Figure 16) to discriminate between H II and AGN dominated systems. All these sources are excluded from the analysis. Additionally two of our normal galaxies (sources #A106, A149; see Fig. A1) are Coma cluster members identified in fields targeting this cluster and are excluded from statistical studies (e.g. $\log N - \log S$, luminosity function).

Table 1 presents our sample including AGNs. We list:

1. Identification number and the NED name of that source if available.
- 2, 3. Right ascension and declination of the optical source in J2000.
4. *B*-band magnitude from the USNO-2 version A2.0.
5. *K*-band magnitude from the 2MASS All Sky Data Release (Skrutskie et al. 1997). Either the extended or the point source catalogue was used.
6. Offset in arcseconds between the X-ray and optical source position.
7. 0.5-2 keV X-ray flux corrected for Galactic absorption in units of $10^{-14} \text{ erg s}^{-1} \text{ cm}^{-2}$.
8. Hardness ratio using the 0.5-2 keV and the 2-4.5 keV spectral bands corrected for vignetting.
9. X-ray-to-optical flux ratio defined in equation 1.
10. 1.4 GHz radio flux density in mJy from either the FIRST (Becker et al. 1995; White et al. 1997) or the NVSS (Condon et al. 1998) surveys.
11. Redshift of the source. In the appendix we present the optical spectra of the normal galaxy candidates in the 1XMM sample obtained at the OAGH and OAN-SPM Mexican telescopes as part of this project.
12. 0.5-2 keV X-ray luminosity in units of erg s^{-1} . For

the k-correction a power-law spectral energy distribution was adopted with photon index $\Gamma = 1.8$.

13. H α luminosity in units of erg s^{-1} . This is measured from the optical spectra after correcting for intrinsic dust obscuration using the Balmer decrement H α /H β . For more details see section 6.

14. 1.4 GHz radio luminosity. For the k-correction a power-law spectral energy distribution was adopted with spectral index $\alpha = 0.8$.

15. Classification on the basis of the optical spectroscopic observations: H II for starforming galaxies, ABS for absorption line spectra and AGN for systems showing evidence for central black hole accretion. There is no spectrum available for source #142 with the redshift estimate, showing both emission and absorption line features, coming from Arp (1977). In the analysis that follows this is assumed to be H II type system.

16. APM star/galaxy separation.

4 THE $\log N - \log S$

The inlet plot in Figure 3 presents the $\log N - \log S$ in the 0.5-2 keV band for our normal galaxy candidates derived using the area curve from section 2.1. The 5 AGNs and the two Coma cluster members in Table 1 are not used in this plot. At faint fluxes ($\lesssim 10^{-14} \text{ erg s}^{-1} \text{ cm}^{-2}$) there is fair agreement with the results from the Needles in the Haystack Survey (NHS; Georgakakis et al. 2004; Georgantopoulos et al. 2005) that used normal galaxies selected in the 0.5-8 keV band. The NHS cumulative counts are shifted to the 0.5-2 keV energy range assuming $\Gamma = 1.8$. At the bright end our counts are elevated compared to this survey, although still consistent within the 1σ uncertainties. This may be because of field-to-field variations affecting primarily the bright flux counts derived from our relatively small area survey ($\approx 6 \text{ deg}^2$). Despite these uncertainties at the bright end, the agreement of our $\log N - \log S$ with previous studies suggests that the area curve derived in section 2.1 is robust.

We improve the statistical reliability of our results by merging our normal galaxy sample with that from the NHS presented by Georgantopoulos et al. (2005). As already mentioned this sample is compiled in the 0.5-8 keV spectral band using public *XMM-Newton* fields overlapping with the SDSS DR-2. A total of 28 systems over $\approx 11 \text{ deg}^2$ are identified. We shift the NHS 0.5-8 keV fluxes and area curve into the 0.5-2 keV band adopting $\Gamma = 1.8$. A total of 13 overlapping fields in the two surveys are taken into account only once in the area curve calculation. The combined sample covers about $\approx 15 \text{ deg}^2$ and comprises a total of 46 unique entries. The $\log N - \log S$ is presented in Figure 3. The differential ‘normal’ galaxy counts in the 0.5-2 keV of the two combined surveys are fit by a power law yielding a slope of -2.46 ± 0.13 . This correspond to a slope of -1.46 ± 0.13 for the cumulative number counts, in agreement with the results of Tajer et al. (2005) at bright fluxes and Hornschemeier et al. (2003; $-1.46^{+0.28}_{-0.30}$) at the faint end, the latter sample based on the same selection criteria used here ($\log f_X/f_{opt} < -2$).

ID	α_{opt} (J2000)	δ_{opt} (J2000)	B (mag)	K (mag)	δ_{XO} ($''$)	$f_X(0.5-2\text{keV})$ ($10^{-14}\text{ erg s}^{-1}\text{ cm}^{-2}$)	HR	$\log f_X/f_{opt}$	$S_{1.4}$ (mJy)	z	$\log L_X(0.5-2\text{keV})$ (erg s^{-1})	$\log L_{H\alpha}$ (erg s^{-1})	$\log L_{1.4\text{ GHz}}$ (W Hz^{-1})	class	photo type
A014	23 04 01.24	+03 15 18.69	13.2	12.54	1.4	3.25 ± 0.33	-0.61 ± 0.06	-2.91	—	—	—	—	—	NONE	GAL
A169	22 28 04.30	-05 17 51.32	16.6	15.24	1.4	0.31 ± 0.05	-0.38 ± 0.13	-2.57	—	—	—	—	—	NONE	GAL
A053	20 39 50.00	-00 59 27.54	12.2	9.55	0.1	1.84 ± 0.24	-0.92 ± 0.05	-3.56	—	0.000	—	—	—	STAR	STAR/GAL
A054	20 39 48.41	-00 56 44.86	15.2	12.48	1.5	0.46 ± 0.12	-1.00 ± 0.30	-2.96	—	0.000	—	—	—	STAR	STAR/GAL
A173	15 04 22.23	+47 41 12.39	15.4	13.08	3.0	0.64 ± 0.11	-1.00 ± 0.08	-2.74	9.53	0.093	41.14	—	23.35	ABS	GAL
A074	13 31 04.83	+24 24 06.84	13.9	<14.47	3.8	0.40 ± 0.07	-0.60 ± 0.10	-3.54	< 1.00	0.028	39.86	40.73	<21.26	HII	GAL
A076	13 30 36.94	+24 22 18.82	13.8	15.15	1.5	0.32 ± 0.07	-0.95 ± 0.13	-3.68	< 1.00	0.031	39.85	40.67	<21.36	HII	GAL
A077	13 29 57.87	+24 11 37.99	17.7	14.09	1.6	0.29 ± 0.08	-1.00 ± 0.32	-2.15	< 1.00	0.165	41.33	—	<22.93	ABS	GAL
A001	13 06 10.88	+18 03 38.58	17.8	15.02	1.7	0.12 ± 0.03	-0.84 ± 0.17	-2.49	< 1.00	0.123	40.69	41.15	<22.65	AGN	GAL
A005	13 05 58.86	+17 57 43.62	16.2	13.97	2.1	0.24 ± 0.04	-0.86 ± 0.15	-2.84	< 1.00	0.080	40.57	—	<22.22	ABS	GAL
A007	13 05 35.27	+18 08 07.34	18.0	14.05	1.2	0.16 ± 0.03	-0.96 ± 0.12	-2.29	< 1.00	0.149	40.99	—	<22.83	ABS	GAL
A006	13 05 20.05	+17 55 22.68	15.1	13.33	1.0	0.18 ± 0.04	-0.86 ± 0.13	-3.40	< 1.00	0.047	39.97	—	<21.73	ABS	GAL
A106, MRK 57	12 58 37.25	+27 10 35.39	12.0	14.30	0.9	0.95 ± 0.18	-0.68 ± 0.11	-3.92	< 1.00	0.026	40.18	—	<21.21	HII	GAL
A149, NGC 4827	12 56 43.59	+27 10 43.44	10.4	11.69	0.6	3.34 ± 0.25	-0.95 ± 0.03	-4.02	11.69	0.024	40.64	—	22.19	ABS	GAL
A171	12 52 05.43	+27 35 47.15	11.7	12.11	2.2	0.28 ± 0.05	-0.56 ± 0.14	-4.57	< 1.00	0.024	39.57	—	<21.12	ABS	GAL
A035	12 49 29.35	-05 57 51.69	18.4	15.07	2.6	0.17 ± 0.05	-0.71 ± 0.27	-2.11	< 1.00	0.199	41.28	—	<23.12	AGN	GAL
A033	12 32 53.13	+64 08 49.74	14.6	12.80	3.1	0.35 ± 0.13	-1.00 ± 0.18	-3.32	2.96	0.076	40.69	—	22.65	ABS	GAL
A146	12 11 17.82	+39 24 29.23	17.1	—	0.3	0.45 ± 0.09	-0.40 ± 0.14	-2.21	< 1.00	0.022	39.71	39.88	<21.06	HII	GAL
A140, NGC 4156	12 10 49.60	+39 28 22.25	10.1	12.20	0.4	12.20 ± 0.19	-0.67 ± 0.01	-3.58	2.93	0.021	41.11	—	21.50	AGN	GAL
A141	12 10 16.62	+39 18 17.01	15.5	12.55	0.4	1.88 ± 0.08	-0.68 ± 0.03	-2.23	< 1.00	0.021	40.29	—	<21.03	ABS	GAL
A142	12 10 13.49	+39 24 32.68	18.8	14.45	0.8	0.07 ± 0.02	-0.53 ± 0.17	-2.32	< 1.00	0.158	40.69	—	<22.89	HII ^a	GAL
A003	11 28 45.86	+58 35 37.15	13.7	<13.31	3.1	0.27 ± 0.06	-0.56 ± 0.19	-3.78	< 1.00	0.059	40.36	40.89	<21.94	HII	GAL
A019	10 44 20.05	-01 24 24.92	17.6	—	2.7	0.15 ± 0.03	-0.37 ± 0.17	-2.47	< 1.00	0.062	40.16	41.00	<21.99	AGN	GAL
A048	10 31 18.94	+31 05 55.65	16.9	13.84	2.3	0.16 ± 0.04	-1.00 ± 0.10	-2.72	< 1.00	0.095	40.58	—	<22.39	ABS	GAL
A111, NGC 3222	10 22 34.51	+19 53 13.30	10.1	10.98	3.5	0.68 ± 0.11	-0.83 ± 0.08	-4.83	< 1.00	0.019	39.75	—	<20.92	ABS	GAL
A011	10 18 31.14	+41 26 43.39	18.1	—	3.8	0.16 ± 0.04	-0.22 ± 0.20	-2.24	< 1.00	0.000	—	—	—	STAR	GAL
A013	10 11 17.55	+55 38 12.81	14.9	13.89	3.2	0.20 ± 0.04	-1.00 ± 0.28	-3.44	2.04	0.118	40.87	41.76	22.92	HII	GAL
A002	10 11 00.93	+55 47 09.90	18.1	15.63	1.9	0.09 ± 0.02	-0.42 ± 0.18	-2.47	< 1.00	0.183	40.96	41.79	<23.04	HII	GAL
A065 MRK 91	08 32 28.19	+52 36 21.39	11.6	11.82	1.5	2.71 ± 0.26	-0.85 ± 0.04	-3.63	12.57	0.016	40.19	41.30	21.86	HII	GAL
A063	08 04 30.49	+64 59 52.43	14.3	10.44	1.2	2.10 ± 0.15	-0.81 ± 0.04	-2.66	39.5	0.149	42.09	—	24.43	AGN	GAL
A031	07 45 50.13	+74 32 57.16	17.3	14.86	1.4	0.40 ± 0.07	-0.53 ± 0.12	-2.18	—	0.000	—	—	—	STAR	STAR/GAL
A044	06 16 12.67	+78 14 31.34	15.9	13.29	1.8	1.28 ± 0.25	-1.00 ± 0.15	-2.24	—	0.067	41.14	—	—	ABS	GAL

The columns are: 1: identification number and common galaxy name if available; 2: right ascension of the optical source; 3: declination of the optical source; 4: optical B -band magnitude; 5: 2MASS K -band magnitude; 6: offset in arcsec between the optical and X-ray source position; 7: X-ray flux in the 0.5-2 keV spectral band in units of $10^{-14}\text{ erg s}^{-1}\text{ cm}^{-2}$; 8: Hardness ratio estimated from the 0.5-2.0 and 2.0-4.5 keV bands; 9: X-ray-to-optical flux ratio; 10: radio flux density; 11: spectroscopic redshift; 12: 0.5-2 keV X-ray luminosity in units of erg s^{-1} ; 13: $H\alpha$ luminosity in units of erg s^{-1} ; 14: 1.4 GHz radio power in units of W/Hz; 15: classification based on optical spectroscopic properties; 16: APM star/galaxy separation on the basis of the optical light profile.

^aThere is no spectrum available for source #142 with the redshift estimate, showing both emission and absorption line features, coming from Arp (1977). In the analysis that follows this is assumed to be HII type system.

Table 1: The candidate ‘normal’ galaxy sample.

5 THE LUMINOSITY FUNCTION

We further explore the statistical properties of the normal galaxy sample by deriving the X-ray luminosity function (LF) using methods that are fully described by Georgantopoulos et al. (2005). We estimate both the binned X-ray LF using the technique of Page & Carrera (2000) and the parametric Maximum Likelihood fit (Tammann, Sandage & Yahil 1979) adopting a Schechter (1976) form for the luminosity function.

We first estimate the 0.5-2 keV LF for the 1XMM data alone. Figure 4 plots our results in comparison with those from the combined NHS and CDF data from Georgantopoulos et al. (2005) shifted to the 0.5-2 keV band assuming $\Gamma = 1.8$. There is good agreement within the 1σ errors further suggesting that the area curve derived in section 2.1 is adequate for statistical studies. We note that the two sources without spectroscopic redshift estimate are not used in this calculation.

We improve the statistical reliability of our LF estimates by combining our sample with both the NHS and 23 $z \lesssim 0.2$ galaxies selected in the 0.5-2 keV spectral band from the CDF-N and CDF-S. The CDF-N data are obtained from Hornschemeier et al. (2003) by selecting a total of 15 sources with 0.5-2 keV band detection. All of these systems have spectroscopic redshifts available. In the case of the CDF-S we select a total of 8 sources detected in the 0.5-2 keV spectral band with $\log f_X/f_{opt} < -2$ from the catalogue presented by Rosati et al. (2001). Spectroscopic (total of 5) or photometric (total of 3) redshifts are available from Szokoly et al. (2004) and Zheng et al. (2004) respectively. This combined sample is also split into absorption and emission line systems to explore the LF for different galaxy types. Our results are plotted in Figure 5 with the maximum likelihood best-fit parameters presented in Table 2, where L_* is the break of Schechter function, α is the faint-end slope and ϕ_* the normalisation. In the same table we give the X-ray emissivity (luminosity per Mpc^3) estimated by the relation $j_x = \int \Phi(L) L dL$, where $\Phi(L)$ is the luminosity function. The 1σ errors on L_* and α are estimated from the regions around the best fit where the likelihood function changes by $\delta L = 0.5$ (e.g. Press et al. 1992). The uncertainties in ϕ_* and j_x are approximated by performing 200 bootstrap resamples of the data and then estimating the 68th percentiles around the median. For a Gaussian distribution these correspond to the 68 per cent confidence level.

Figure 5 also compares the X-ray luminosity function of the combined 1XMM+NHS+CDF sample at a mean redshift $z = 0.087$ with the higher- z LF estimates of Norman et al. (2004). These authors used Bayesian statistical analysis to select normal galaxy candidates in the CDF-North and South and derived the first ever X-ray luminosity function for these systems in two redshift bins with medians $z = 0.26$ and $z = 0.66$ respectively. Their $z < 0.5$ LF in Figure 5 is in fair agreement with ours at the faint end but diverges at brighter luminosities. This may suggest (i) contamination of the Norman et al. (2004) sample by AGNs at bright luminosities, (ii) bias in our sample against X-ray ultra-luminous systems (e.g. $L_X \gtrsim 10^{42} \text{ erg s}^{-1}$) because of the $\log(f_X/f_{opt}) < -2$ selection or (iii) evolution of the normal galaxy luminosity function. In the latter case, the median redshift of the $z < 0.5$ subsample of Norman et al.

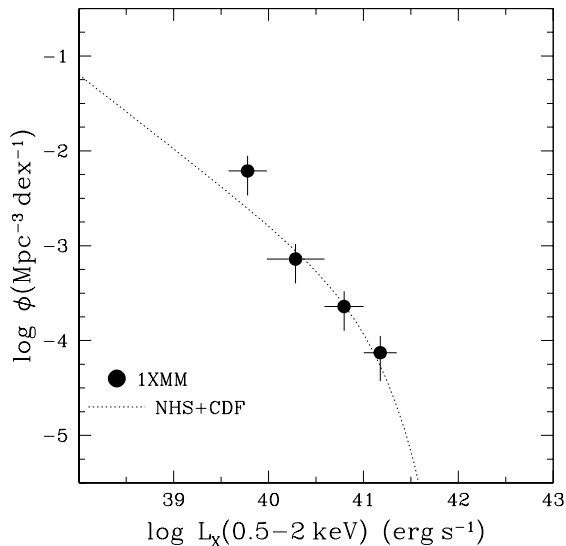


Figure 4. The local 0.5-2 keV luminosity function for the present sample of 1XMM galaxies. Also shown is the maximum likelihood fit method for $z < 0.2$ normal galaxies from the combined NHS and CDF samples (see Georgantopoulos et al. 2005) shifted from the 0.5-8 to the 0.5-2 keV band assuming $\Gamma = 1.8$.

is $z_{median} = 0.26$ higher than our mean of $z = 0.087$. For luminosity evolution of the form $(1+z)^{2.7}$ derived by Norman et al. (2004), a source at $z = 0.26$ is expected to become about 1.5 times more luminous relative to $z = 0.087$. Such a brightening can indeed, partially account for the observed differences.

In Table 2 we also estimate a 0.5-2 keV X-ray emissivity of $(0.24 \pm 0.02) \times 10^{38}$ and $(0.22 \pm 0.03) \times 10^{38} \text{ erg s}^{-1} \text{ Mpc}^{-3}$ for emission and absorption line systems respectively. These values are lower than previous estimates. For example Georgakakis et al. (2003b) used stacking analysis to estimate the mean X-ray properties of 2dF galaxies at $z \approx 0.1$. These authors estimate $j_X = (0.4 \pm 0.3) \times 10^{38}$ and $(1.2 \pm 0.4) \times 10^{38} \text{ erg s}^{-1} \text{ Mpc}^{-3}$ for late and early type galaxies respectively. Georgantopoulos, Basilakos & Plionis (1999) convolved the local optical luminosity function of the Ho, Filippenko & Sargent (1997) sample with the corresponding $L_X - L_B$ relation based on *Einstein* data. Their j_X estimates scaled to the 0.5-2 keV band are $(0.50 \pm 0.06) \times 10^{38} \text{ erg sec}^{-1} \text{ Mpc}^{-3}$ for H II galaxies and $(0.53 \pm 0.06) \times 10^{38} \text{ erg sec}^{-1} \text{ Mpc}^{-3}$ for passive galaxies. The origin of the discrepancy between the emissivity estimates presented here and those found in the studies above is not clear. In the case of stacking analysis for example, luminous systems may bias the mean signal toward high values, resulting in an overestimation of the j_X . Although the method presented here for estimating j_X is direct and robust, we note that a possible bias in our sample against high L_X systems may result in a systematic reduction of the j_X .

Sample	Number of sources	mean redshift	$\log L_*$ (erg s^{-1})	α	ϕ_* ($\times \ln(10) \times 10^{-4} \text{ Mpc}^{-3} \text{ dex}^{-1}$)	j_x ($\times 10^{38} \text{ erg s}^{-1} \text{ Mpc}^{-3}$)
1XMM/NHS/CDF	67*	0.087	$41.02^{+0.14}_{-0.12}$	$-1.76^{+0.10}_{-0.10}$	$3.4^{+2.5}_{-1.8}$	$0.47^{+0.04}_{-0.04}$
Emission	33	0.091	$40.65^{+0.17}_{-0.14}$	$-1.61^{+0.20}_{-0.17}$	$6.0^{+7.3}_{-3.8}$	$0.24^{+0.02}_{-0.02}$
Absorption	34	0.083	$41.25^{+0.25}_{-0.18}$	$-1.79^{+0.13}_{-0.14}$	$0.9^{+1.1}_{-0.4}$	$0.22^{+0.03}_{-0.03}$

*The 2 sources in the 1XMM sample without redshift determination have been excluded from the analysis.

Table 2. The luminosity function best-fit parameters

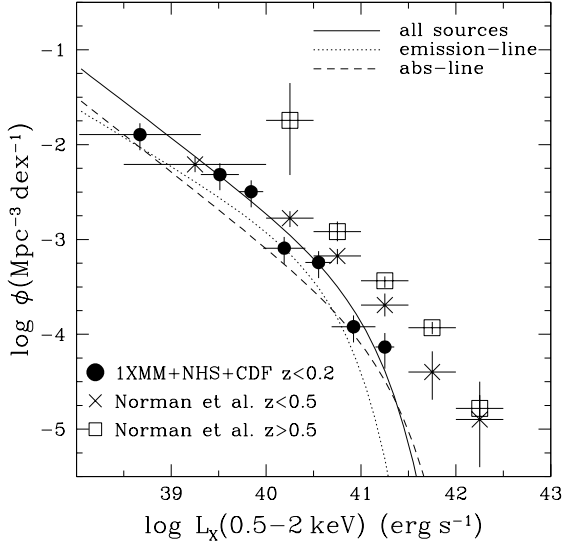


Figure 5. The 0.5-2 keV luminosity function for the combined sample of 1XMM, NHS and CDF $z < 0.2$ normal galaxies. The derived maximum-likelihood fits to the observations are shown with the continuous (full sample), dotted (emission-line objects) and dashed (absorption-line systems) lines. For clarity the results from the non-parametric method are shown with filled circles only for the full sample. The luminosity function derived by Norman et al. (2004) in two redshift bins is plotted for comparison.

6 X-RAY LUMINOSITY AND HOST GALAXY PROPERTIES

Using the 1XMM+NHS sample we explore the correlation between 0.5-2 keV X-ray luminosity and indicators of star-formation activity. The $H\alpha$ luminosity ($L_{H\alpha}$) measured from the optical spectra and the 1.4 GHz radio luminosity ($L_{1.4}$) obtained from either the FIRST or the NVSS surveys are used as proxies to the galaxy SFR. Only X-ray selected normal galaxy candidates with emission line optical spectra are considered here.

Figure 6 plots L_X against $L_{1.4}$ for our sources. Because of the large number of upper limits we do not attempt to fit an $L_X - L_{1.4}$ relation to the data. Also shown in this figure for comparison are the spiral galaxies from Shapley et al. (2001). These authors compiled an optically selected sample of local spirals with X-ray data (detections or upper limits) from the *Einstein* observatory and 4.85 GHz radio flux densities from the literature. Powerful AGNs in this sample are not plotted in Figure 6. The *Einstein* X-ray fluxes in the 0.2-4 keV band are transformed to the 0.5-2 keV band assuming a power-law model with a spectral index $\Gamma = 1.8$. At

radio wavelengths a power-law spectral energy distribution of the form $f_\nu \sim \nu^{-0.8}$, appropriate for star-forming galaxies, is adopted to convert the 4.85 GHz radio flux density of Shapley et al. (2001) to 1.4 GHz. Also shown in this plot is the $L_X - L_{1.4}$ relation of Ranalli et al. (2003) of the form $L_X \propto L_{1.4}^{0.88}$. These authors used *ASCA* and *BeppoSAX* data of optically selected star-forming galaxies classified on the basis of high quality nuclear spectra from Ho et al. (1997). Many of our sources are not detected at 1.4 GHz to the 1 mJy flux density limit of the FIRST survey. The upper limits and detections, although within the scatter of the Shapley et al. (2001) data, appear slightly offset from the Ranalli et al. (2003) best-fit relation, particularly for star-formation rates $< 10 M_\odot \text{ yr}^{-1}$. This may suggest a contribution from low-mass X-ray binaries (e.g. old stellar population) to the observed X-ray emission of more quiescent systems. A larger number of radio detections is required to further explore this issue.

In Figure 7 we plot L_X against $H\alpha$ luminosity for emission-line galaxies in the combined 1XMM+NHS sample only. The latter is measured from the optical spectra after correcting for intrinsic dust obscuration. We quantify the visual extinction, A_V , by comparing the $H\alpha/H\beta$ decrement with the theoretical (case B recombination) value of 2.86 (Brocklehurst 1971) and a standard reddening curve (Savage & Mathis 1979). The technique is hampered by the poor S/N ratio of some of the spectra and by stellar $H\beta$ absorption that reduces the measured flux of this line. We account for this effect by applying a correction of -2 \AA to $H\beta$, similar to the mean stellar absorption in this line determined for star-forming galaxies (Tresse et al. 1996; Georgakakis et al. 1999). A small number of systems in our sample have $H\alpha/H\beta$ ratios below the theoretical value of 2.86 for case B recombination, suggesting either little dust reddening, stellar $H\beta$ absorption lower than -2 \AA or poor signal-to-noise ratio optical spectra. For these sources we still apply a correction to $H\alpha$ for dust obscuration adopting the mean optical extinction of $A_V = 1$ mag for spiral galaxies determined by Kennicutt (1992).

The best-fit relation of the form $L_X \propto L_{H\alpha}^\beta$ with $\beta = 0.69 \pm 0.06$ is plotted in Figure 7. This is estimated using the bisector least square fitting described in Isobe et al. (1990). Also shown is the $L_X - L_{H\alpha}$ relation for star-forming galaxies determined by Zezas (2000) using a total of 43 systems with PSPC ROSAT data, classified as H II on the basis of high quality nuclear optical spectra from Ho et al. (1997). The exponent of the Zezas (2000) relation is $\beta = 0.62 \pm 0.11$ in good agreement with our determination. There is however a difference in the normalisation. This is most likely because Zezas (2000) uses $H\alpha$ luminosities integrated over the whole galaxy whereas we are measuring this

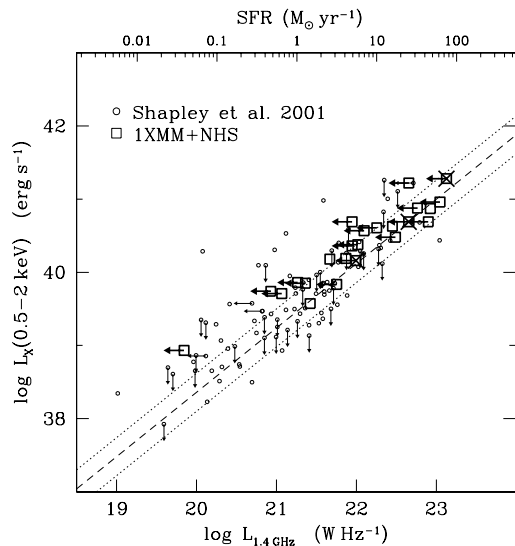


Figure 6. 0.5-2 keV X-ray luminosity against radio power. The $L_{1.4}$ is converted into SFR on the top horizontal axis using the relation of Bell et al. (2003). The large open squares are the emission-line galaxies from the 1XMM+NHS sample. A cross on top of a symbol is for AGNs. Radio upper limits are shown with an arrow pointing to the left. The small open circles are local spiral galaxies from Shapley et al. (2001). The dashed line is the best fit $L_X - L_{1.4}$ relation of the form $L_X \propto L_{1.4}^{+0.88}$ derived by Ranalli et al. (2003). The dotted lines represent the 1 sigma rms envelope around the best fit.

line through a slit (or a fibre in the case of SDSS data) with typical angular size of 2 arcsec. This width corresponds to a physical scale of about 2 kpc diameter at the mean redshift of our sample. Extrapolating fluxes measured through a slit to integrated values over the whole galaxy is not straightforward and depends on the size of star-forming regions, their distribution in the galaxy, the position of the slit and the seeing at the time of the observations.

We further explore the association between 0.5-2 keV X-ray luminosity and galaxy mass for absorption-line galaxies in the combined 1XMM+NHS sample. The K -band luminosity is used as proxy to the stellar mass of the system. Figure 8 plots L_X against L_K . Also shown in this figure is the relation between the total X-ray luminosity of point sources, L_{XP} , and the host galaxy L_K determined by Colbert et al. (2004) using Chandra observations of nearby ellipticals. This line shows the mean expected contribution of low-mass X-ray binaries to the observed emission at a given K -band luminosity or galaxy mass and does not include the X-ray emitting hot gas component.

For absorption-line systems in our sample (excluding AGNs) we adopt a relation of the form $L_X \propto L_K^\gamma$ to estimate a bisector exponent $\gamma = 1.5 \pm 0.1$. This is flatter than the slope of ≈ 1.8 found by Fabbiano et al. (1992) for the $L_X - L_B$ relation of local E/S0s and Hornschemeier et al. (2005) for the L_X /stellar-mass correlation of absorption line galaxies in the SDSS. This apparent discrepancy may be due to the $\log f_X/f_{opt} < -2$ cutoff that effectively excludes from the sample very luminous X-ray selected normal galaxies. For example about 20 per cent of the Fabbiano et al. (1992) sample have $\log L_X/L_B > -2$. The vast majority of these

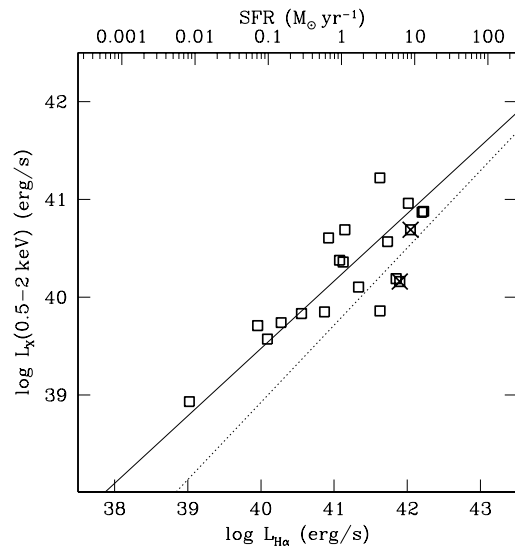


Figure 7. 0.5-2 keV X-ray luminosity against $H\alpha$ luminosity corrected for intrinsic dust obscuration for the combined 1XMM+NHS emission-line galaxies. The $H\alpha$ is converted into SFR on the top horizontal axis using the relation of Kennicutt (1998). A cross on top of a symbol is for AGNs. The continuous line shows the bisector least squares fit relation of the form $L_X \propto L_{H\alpha}^\beta$ with $\beta = 0.69 \pm 0.06$. The dotted line is the $L_X - L_{H\alpha}$ relation for star-forming galaxies of Zezas (2000). Although the slopes of the two lines are similar they differ in the normalisation. This is most likely because Zezas (2000) used $H\alpha$ data integrated over the whole galaxy rather than slit spectroscopy used here.

systems are also luminous with $L_X \gtrsim 10^{42}$ erg s $^{-1}$. Excluding E/S0 galaxies with $\log L_X/L_B > -2$ from that sample we find a flatter slope of ≈ 1.5 for the $L_X - L_B$ relation in agreement with the value estimated here. Alternatively the flatter $L_X - L_K$ relation may indicate that the K -band provides a better proxy to galaxy mass. For example, Shapley et al. (2001) used H -band near-infrared data and find a flatter slope for the $L_X - L_H$ relation of spirals compared to the $L_X - L_B$ relation for the same systems. Although comparing the X-ray properties of ellipticals and spirals is not appropriate it suggests that the flatter slope we are estimating may be partly due to the use of near-infrared rather than optical luminosities.

7 SUMMARY AND CONCLUSIONS

In this paper we demonstrate the power of the First *XMM-Newton* Serendipitous Source Catalog for studies of X-ray selected normal galaxies. Our sample is compiled from X-ray sources detected on *XMM-Newton* pointings that have (i) EPIC-PN detector as prime instrument operated in full-frame mode, (ii) exposure time > 7 ks, (iii) declinations $\text{DEC}(J2000) > -10$ deg, (iv) galactic latitude $|\text{b}_{\text{II}}| > 20$ deg and (v) right ascension $\text{RA}(J2000) > 4$ hours. A total of 51 fields fulfil the above criteria, covering a total area of ≈ 6 deg 2 to the 0.5-2 keV band limit $f_X(0.5 - 2 \text{ keV}) \approx 10^{-15}$ erg s $^{-1}$ cm $^{-2}$.

The USNO A2.0 catalogue provides a homogeneous platform that allows identification of X-ray selected normal

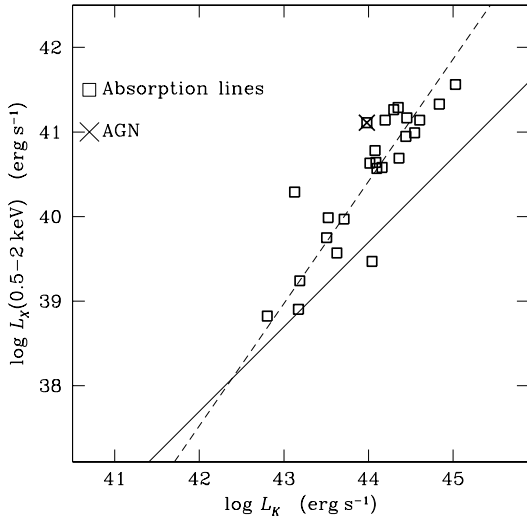


Figure 8. 0.5-2 keV X-ray luminosity against K -band luminosity. The large squares are normal galaxies in the NHS and 1XMM samples with absorption line optical spectra. A cross on top of a symbol is for sources in our sample that show evidence for AGN activity. The continuous line is the $L_X - L_K$ relation of Colbert et al. (2004) which, for a given K -band luminosity, corresponds to the mean expected contribution of the point source X-ray binary population to L_X . The dashed line is the best fit relation to absorption line galaxies in our combined NHS+1XMM sample.

galaxy candidates on the basis of the low X-ray-to-optical flux ratios of these sources, $\log f_X/f_{opt} < -2$. Reliable star/galaxy separation is available from the APM, allowing us to exclude Galactic stars that also have $\log f_X/f_{opt} < -2$. Optical spectroscopy is then used to identify systems that show evidence for AGN activity resulting in a sample of 23 normal galaxy candidates: 9 with narrow emission lines, 12 with absorption lines only and 2 without optical spectroscopic information. Future releases of the *XMM-Newton* Serendipitous Source Catalog will provide much wider areal coverage resulting in significantly larger low- z normal galaxy samples.

At present we increase our sample size by combining it with X-ray selected normal galaxy candidates from the Needles in the Haystack Survey (Georgantopoulos et al. 2005). This provides a total of 46 $z \lesssim 0.2$ X-ray detected normal galaxies, the largest low- z sample yet available. Such a large number of sources provides a unique opportunity to constrain the normal galaxy $\log N - \log S$ at bright fluxes ($10^{-15} - 10^{-13} \text{ erg s}^{-1} \text{ cm}^{-2}$). We estimate a slope of -1.46 ± 0.13 consistent with the euclidean prediction and in agreement with previous determinations (Hornschemeier et al. 2003; Tajer et al. 2005).

Our enlarged sample is further combined with 23 local ($z \lesssim 0.2$) galaxies from the *Chandra* Deep Field North and South surveys to construct the local X-ray luminosity function of normal galaxies. This is fit with a Schechter function with a break at $\log L_* = 41.02^{+0.14}_{-0.12} \text{ erg s}^{-1}$ and a slope of $\alpha = -1.76 \pm 0.10$. The large sample size allows us to also estimate the luminosity function of emission and absorption line systems separately and to provide the most accurate es-

timates of the 0.5-2 keV X-ray emissivity of these systems in the nearby Universe. We find $j_X = (0.24 \pm 0.02) \times 10^{38}$ and $(0.22 \pm 0.03) \times 10^{38} \text{ erg s}^{-1} \text{ Mpc}^{-3}$ for emission and absorption line systems respectively. We note that these are lower than previous (less direct) estimates based on stacking analysis (e.g. Georgakakis et al. 2003b) or optically selected local galaxies (Georgantopoulos et al. 1999).

Finally, for the combined sample of 46 systems we explore the association between X-ray luminosity and host galaxy properties, such as SFR and stellar mass. We use the 1.4 GHz radio and $H\alpha$ luminosities as star-formation indicators. We find that the $L_X - L_{1.4}$ relation for our sources is consistent with that determined by Ranalli et al. (2003) for the local Universe. For the $\log L_X - \log L_{H\alpha}$ correlation we estimate a slope of ≈ 0.7 in fair agreement with previous results (Zezas 2000). The above relations suggest that the X-ray luminosity in the emission-line galaxies in our sample is directly related to the current star-formation activity as measured by the 1.4 GHz radio and $H\alpha$ luminosities. For the early type galaxies in the sample showing absorption optical lines only we use the K -band as proxy to their stellar mass and find a linear correlation between $\log L_X$ and $\log L_K$ with a slope of ≈ 1.5 . This is flatter than the slope of ≈ 1.8 for the $L_X - L_B$ relation for local ellipticals of Fabbiano et al. (1992) or the L_X /stellar-mass correlation for absorption line galaxies in the SDSS determined by Hornschemeier et al. (2005). This may be due to a possible bias in our sample against very luminous galaxies, $L_X > 10^{42} \text{ erg s}^{-1} \text{ cm}^{-2}$, likely introduced by the low X-ray-to-optical flux ratio selection. Alternatively, this may indicate that the K -band provides a better representation of the galaxy mass.

8 ACKNOWLEDGMENTS

We thank the anonymous referee for valuable comments that significantly improved this paper. AG acknowledges funding by the European Union and the Greek Ministry of Development in the framework of the programme ‘Promotion of Excellence in Technological Development and Research’, project ‘X-ray Astrophysics with ESA’s mission XMM’. We acknowledge the use of data from the *XMM-Newton* Science Archive at VILSPA. VC acknowledges the CONACYT research grant 39560-F.

Funding for the creation and distribution of the SDSS Archive has been provided by the Alfred P. Sloan Foundation, the Participating Institutions, the National Aeronautics and Space Administration, the National Science Foundation, the U.S. Department of Energy, the Japanese Monbukagakusho, and the Max Planck Society. The SDSS Web site is <http://www.sdss.org/>. The SDSS is managed by the Astrophysical Research Consortium (ARC) for the Participating Institutions. The Participating Institutions are The University of Chicago, Fermilab, the Institute for Advanced Study, the Japan Participation Group, The Johns Hopkins University, Los Alamos National Laboratory, the Max-Planck-Institute for Astronomy (MPIA), the Max-Planck-Institute for Astrophysics (MPA), New Mexico State University, University of Pittsburgh, Princeton University, the United States Naval Observatory, and the University of Washington.

APPENDIX A:

In this appendix we present the optical spectra of the normal galaxy candidates in the 1XMM sample obtained at the OAGH and OAN-SPM Mexican telescopes as part of this project.

REFERENCES

- Alexander D., et al., 2003, *AJ*, 126, 539
- Alexander D. M., Aussel H., Bauer F. E., Brandt W. N., Hornschemeier A. E., Vignali C., Garmire G. P., Schneider D. P., 2002, *ApJ*, 568L, 85
- Arp H., 1977, *ApJ*, 218, 70
- Baldi A., Molendi S., Comastri A., Fiore F., Matt G., Vignali C., 2002, *ApJ*, 564, 190
- Baldwin J. A., Phillips M. M., Terlevich R., 1981, *PASP*, 93, 5
- Bauer F. E., Alexander D. M., Brandt W. N., Hornschemeier A. E., Vignali C., Garmire G. P., Schneider D. P., 2002, *AJ*, 124, 2351
- Becker R. H., White R. L., & Helfand D. J., 1995, *ApJ*, 450, 559
- Bell E. F., 2003, *ApJ*, 586, 794
- Brocklehurst M., 1971, *MNRAS*, 153, 471
- Condon J. J., Cotton W. D., Greisen E. W., Yin Q. F., Perley R. A., Taylor G. B., & Broderick J. J., 1998, *AJ*, 115, 1693
- Colbert E. J. M., Heckman T. M., Ptak A. F., Strickland D. K., Weaver K. A., 2004, *ApJ*, 602, 231
- Elvis M., Schreier E. J., Tonry J., Davis M., Huchra J. P., 1981, *ApJ*, 246, 20
- Fabbiano G., Kim, D.W., Trinchieri, G., 1992, *ApJS*, 80, 531
- Gallagher S. C., Brandt W. N., Sambruna R. M., Mathur S., Yamasaki N., 1999, *ApJ*, 519, 549
- Georgakakis, A.E., Georgantopoulos, I., Basilakos, S., Plionis, M., Kolokotronis, V., 2004, *MNRAS*, 354, 123
- Georgakakis A., Hopkins A. M., Sullivan M., Afonso J., Georgantopoulos I., Mobasher B., Cram L. E., 2003a, *MNRAS*, 345, 939
- Georgakakis A., Georgantopoulos I., Stewart G. C., Shanks T., Boyle B. J., 2003b, *MNRAS*, 344, 161
- Georgakakis A., Mobasher B., Cram L., Hopkins A., Lidman C., Rowan-Robinson M., 1999, *MNRAS*, 306, 708
- Georgantopoulos I., Georgakakis A., Koulouridis E., 2005, *MNRAS*, in press, astro-ph/0503494
- Georgantopoulos I., Basilakos S., Plionis M., 1999, *MNRAS*, 305, L31.
- Ho L. C., Filippenko A. V., Sargent W., 1997, *ApJS*, 112
- Hopkins, A., 2004, *ApJ*, 615, 209
- Hornschemeier A. E., Heckman T. M., Ptak A. F., Tremonti C. A., Colbert E. J. M., 2005, *AJ*, in press, astro-ph/0410669
- Hornschemeier A. E. et al., 2003, *AJ*, 126, 575
- Hornschemeier A. E., Brandt W. N., Alexander D. M., Bauer F. E., Garmire G. P., Schneider D. P., Bautz M. W., Chartas G., 2002, *ApJ*, 568, 82.
- Isobe T., Feigelson E. D., Akritas M. G., Babu G. J., 1990, *ApJ*, 364, 104
- Kennicutt R. C. Jr., 1998, *ARA&A*, 189
- Kennicutt R. C. Jr., 1992, *ApJ*, 388, 310
- Kewley L. J., Dopita M. A., Sutherland R. S., Heisler C. A., Trevena J., 2001, *ApJ*, 556, 121
- Laird E. S., Nandra K., Adelberger K. L., Steidel C. C., Reddy N. A., *MNRAS*, in press, astro-ph/0501411
- Monet D. G., et al., 2003, *AJ*, 125, 984
- Nandra K., Mushotzky R. F., Arnaud K., Steidel C. C., Adelberger K. L., Gardner J. P., Teplitz H. I., Windhorst R. A., 2002, *ApJ*, 576, 625
- Norman C., et al., 2004, *ApJ*, 607, 721
- Page, M.J. & Carrera, F.J. 2000, *MNRAS*, 311, 433
- Ranalli, P., Comastri, A. Setti, G., 2003, *A&A*, 399, 39
- Savage B. D., & Mathis J. S., 1979, *ARA&A*, 17, 73
- Shapley A., Fabbiano G., Eskridge P. B., 2001, *ApJS*, 137, 139
- Schechter, P., 1976, *ApJ*, 203, 297
- Skrutskie M. F. et al., 1997, conf. proceedings on "The Impact of Large Scale Near-IR Sky Surveys", eds. F. Garzon et al., p. 25., Kluwer Academic Publishing Company
- Stocke, J.T. et al., 1991, 76, 813
- Stoughton C., et al., 2002, *AJ*, 123, 485.
- Strüder L., Briel U., Dennerl K., et al. 2001, *A&A*, 365, L18.
- Szokoly G. P., et al., 2004, *ApJS*, 155, 271
- Tajer M., Trinchieri G., Wolter A., Campana S., Moretti A., Tagliaferri G., 2005, *A&A*, in press, astro-ph/0412588
- Takeuchi, T.T., Yoshikawa, K.I., Takako T., 2003, *ApJ*, 587, L89
- Tammann, G.A., Yahil, A., Sandage, A., 1979, *ApJ*, 234, 775
- Tresse L., Rola C., Hammer F., Stasinska G., Le Fevre O., Lilly S. J., Crampton D., 1996, *MNRAS*, 281, 847
- Turner M. J. L., Abbey A., Arnaud M., et al., 2001, *A&A*, 365, L27.
- Veilleux S. & Osterbrock D. E., 1987, *ApJS*, 63, 295
- White R. L., Becker R. H., Helfand D. J., & Gregg M. D., 1997, *ApJ*, 475, 479
- York D. G., et al., 2000, *AJ*, 120, 1579
- Zeas A., 2000, PhD Thesis, University of Leicester
- Zheng W., et al., 2004, *ApJS*, 155, 73Z
- Zickgraf F.J., Thiering I., Krautter J., et al. 1997, *A&AS*, 123, 103

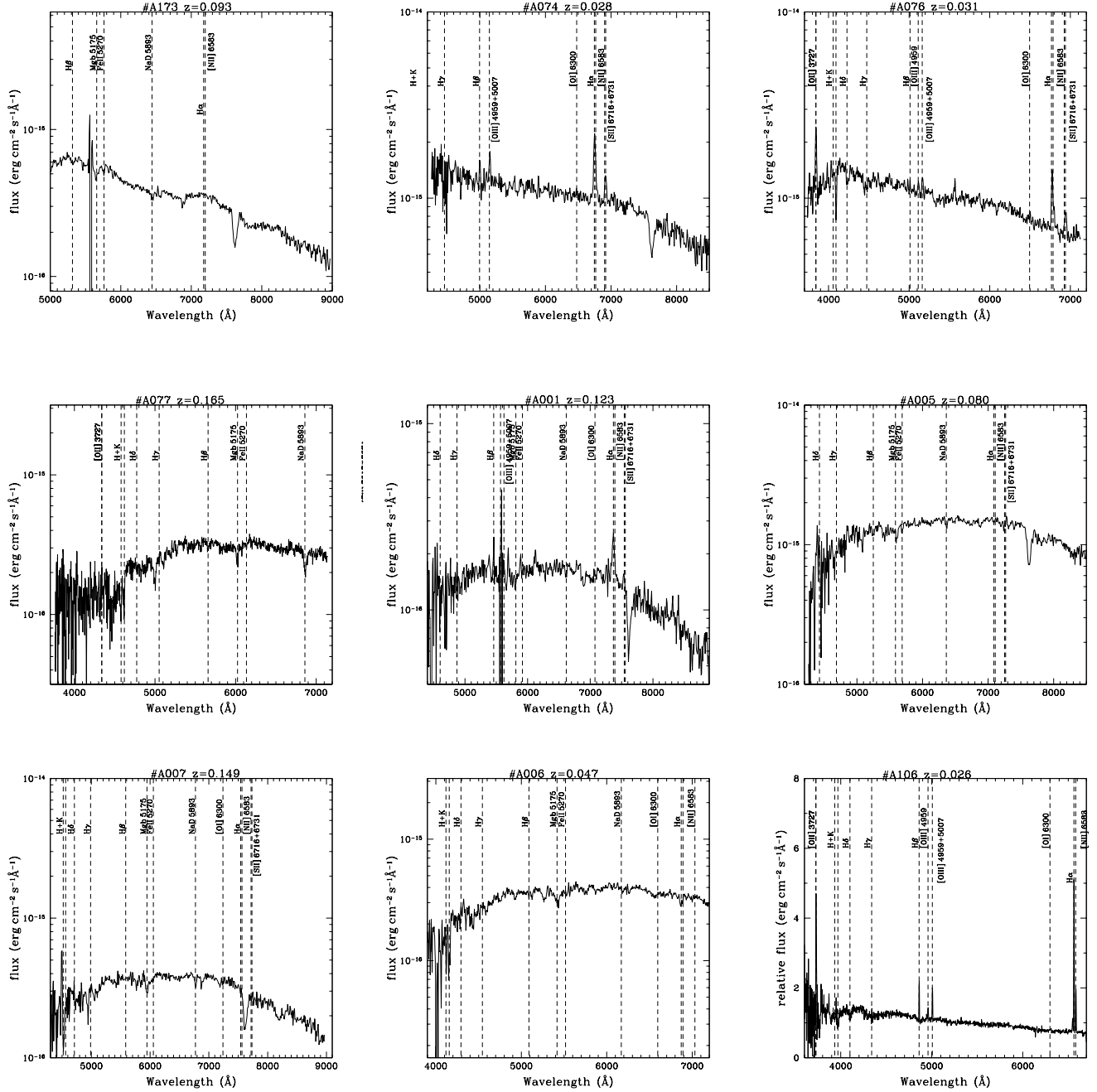


Figure A1. Optical spectra of galaxy candidates in the 1XMM sample obtained at the OAGH and OAN-SPM Mexican telescopes. Sources A001, A035 and A019 are classified AGN.

Figure A1 – continued

